特集 15
研究速報

Numerical Simuration Of Complex Turbulent Jets: Origin Of Axis-Switching

複雑乱流噴流の数値シミュレーション（軸伸張の発生）

Ayodeji O. DEMUREN*, Robert V. WILSON** and Toshio KOBAYASHI*
アヨデシ　オー　デムレン・ロバート　ヴィ　ウィルソン・小　林　敏　雄

INTRODUCTION

Turbulent jets are present in many physical processes and technological applications. In most cases, efficient mixing of the jets with ambient fluid is desired. Experiments [1-4] have shown that three-dimensional (3-D) jets can be used to enhance mixing and entrainment rates in comparison to nominally two-dimensional (2-D), plane or axi-symmetric, jets. A fundamental understanding of the dynamics of complex, turbulent jets is required for their prediction and control. The present study is concerned with the understanding of the roles of vorticity and turbulence in the spatial evolution of incompressible 3-D jets in the near to medium field and the effects of external forcing and Reynolds number thereupon.

Some analytical studies have used vortex-induction arguments [5, 6] or stability analysis [7, 8] to explain some observed phenomena in complex jets, such as axis-switching and enhanced mixing. In the former category, the Biot-Savart law was used to predict how elliptic vortex rings would distort and switch axes. Jets are of course not vortex rings. On the other hand, conventional RANS approach by McGuirk and Rodi [9] failed to predict observed axis-switching and saddle-shaped velocity profiles in turbulent rectangular jets.

MATHEMATICAL FORMULATION

Governing Equations

The partial differential equations governing the incompressible jet fluid flow are the Navier-Stokes equations which can be written in Cartesian tensor form, for dimensionless variables as:

$$\frac{\partial u_i}{\partial t}+u_j\frac{\partial u_i}{\partial x_j}=-\frac{\partial p}{\partial x_i}+\frac{1}{Re_D}\frac{\partial^2 u_i}{\partial x_j\partial x_j} \quad \cdots\cdots\cdots\cdots (1)$$

where, u_i are the Cartesian velocity components in the Cartesian coordinate directions x_i, p is the pressure and Re_D is the Reynolds number based on the equivalent diameter. These equations must be solved in conjuction with the continuity equation:

$$\frac{\partial u_i}{\partial x_i}=0 \quad \cdots\cdots\cdots\cdots\cdots\cdots\cdots\cdots\cdots\cdots (2)$$

which expresses the divergence-free velocity condition.

At higher Reynolds numbers, all scales present in the flow cannot be resolved on computational grids that present resources would allow, so a large eddy simulation (LES) must be uti-lized. The application of a grid filter, $\bar{G}$, to equations (1) and (2) results in the filtered equations of motion:

$$\frac{\partial \bar{u}_i}{\partial t}+\bar{u}_j\frac{\partial \bar{u}_i}{\partial x_j}=-\frac{\partial}{\partial x_i}\bar{P}+\frac{1}{Re_{D_e}}\frac{\partial^2 \bar{u}_i}{\partial x_j\partial x_j}-\frac{\partial \tau_{ij}}{\partial x_j} \quad \cdots\cdots (3)$$

and

$$\frac{\partial \bar{u}_i}{\partial x_i}=0 \quad \cdots\cdots\cdots\cdots\cdots\cdots\cdots\cdots\cdots\cdots (4)$$

which $\tau_{ij}=\overline{u_iu_j}-u_iu_j$ is the subgrid scale (SGS) stress which must be modeled in terms of the resolved velocity field. The Smagorinsky eddy-viscosity model is utilized in the present study to apporoximate the SGS stress as:

$$\tau_{ij}-\frac{\delta_{ij}}{3}\tau_{kk}=-2C_s\bar{\Delta}^2|\bar{S}|\bar{S}_{ij} \quad \cdots\cdots\cdots\cdots\cdots (5)$$

where $\bar{\Delta}$ is a length scale associated with the grid size, $\bar{S}_{ij}=\frac{1}{2}\left(\frac{\partial \bar{u}_i}{\partial x_j}+\frac{\partial \bar{u}_j}{\partial x_i}\right)$ is the resolved strain rate tensor, and $|\bar{S}|=\sqrt{2\bar{S}_{ij}\bar{S}_{ij}}$ .The models coefficient, C_s, is set to the constant value of 0.01. Time-averaged budget of Eq. (3),suggests that this treatment is adequate since the SGS stress is considerably smaller than the resolved Reynolds stress.

The Navier-Stokes Eq. (1) or the filtered Eq. (3) are dis-

* Center for collaborative Reserch, University of Tokyo
** Department of Mechanical Engineering, Old Dominion University

cretized temporally with an explicit third-order Runge-Kutta (RK) scheme and spatially with implicit fourth-order compact finite difference schemes [10].

MODEL PROBLEMS

Spatial simulations of various 3D jet flows are performed in this study in which a fixed region of the flow is computed and disturbances grow in the streamwise direction. Table 1 summarizes the test cases. Discrete or broad made instabilities are present in the shear layers [11].

All computations are performed on a 10^3 domain, with 104x 128^2 uniform grid points in the streamwise and cross-plane directions, respectively. In all cases, D_e =1. Additional 24 streamwise grid points lie in a 2 diameter long buffer zone.

RESULTS AND DISCUSSION

Low Reynolds Number Jets

Figures 1 to 3 show computed instantaneous vorticity fields for the low Reynolds number cases 1 to 3, respectively. In case 1, the flow remains symmetrical about the major and minor axes,

Table 1.　Parameter for Test Cases

Test Case	Re_D	Jet Geometry	Shear-Layer Instability Mode	DNS or LES
1	750	2:1 Rectangular	Fundamental	DNS
2	750	2:1 Rectangular	Fundamental + 1st sub-Harmonic	DNS
3	750	2:1 Rectangular	Broad	DNS
4	75,000	2:1 Rectangular	Broad	LES
5	75,000	2:1 Elliptic	Broad	LES
6	75,000	Circular	Broad	LES

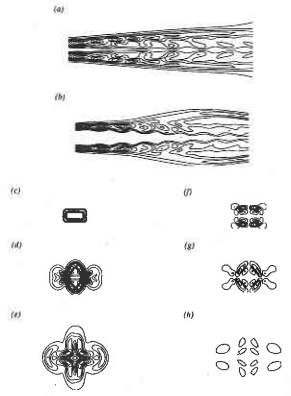

Figure 1.　Contours of vorticity magnitude, (a)-(e) and streamwise vorticity, (f)-(h) for case 1 at t = flow through 2 times, for fundamental forcing function. (a) minor axis plane, z/D_e = 0, (b) major axis plane, y/D_e = 0, (c) cross flow plane, x/D_e = 0, (d) x/D_e = 5, (e) x/D_e = 10, (f) x/D_e = 2.5, (g) x/D_e = 5, and (h) x/D_e = 10.

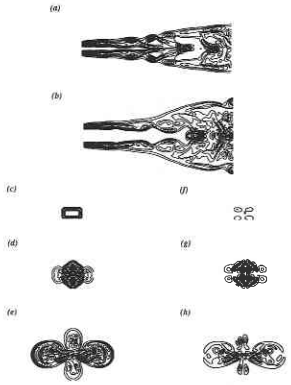

Figure 2.　Contours of vorticity magnitude, (a)-(e) and streamwise vorticity, (f)-(h) for case 2 (see Fig 1. for legend)

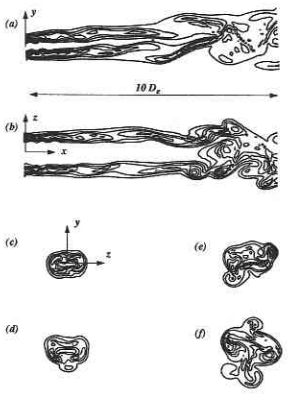

Figure 3.　Countours of vorticity for case (3) at t = 2 flow through times for broad mode forcing function. (a) minor axis plane, z/D_e= 0, (b) major axis plane, y/D_e = 0, (c) cross flow plane, x/D_e = 2.5, (d) x/D_e = 5, (e) x/D_e = 7.5, and (f) x/D_e = 10.

just like the inlet mean flow and perturbation velocities, hence the flow has remained laminar and transition to turbulence did not occur in the 10 diameters computed. The phenomenon of axis switching is observed to be taking place near the end of the domain. The source of this is seen to be clearly in the complex vorticity field. It is most likely due to self-induction, since there is no streamwise vorticity at the inlet plane. It appears that the effect of the induced streamwise vorticity field is to pump fluid from the major axis to the minor axis. This process can be explained with deformation of vortex rings [6]. Spanwise rollers are seen in Figs. 1 (a) and (b) which form super-elliptical vortex rings. Through self-induction, the narrow ends will move faster in the streamwise direction than the wider sides; a process which will eventually lead to axis-switching. In case 2, the vortex field is even more complex. Self-induction must now compete with the instability mechanism which produces vortex pairing in 2D mixing layers. In the latter (see Wilson and

Demuren [11]), the presence of the sub-harmonic disturbance mode produces a transverse shift, into faster moving fluid, in every other spanwise roller which eventually catches up with the preceding roller and pairs with it. The effect of this process, in this 3D case, is that two subsequent vortex rings now have different shapes and the interaction between them produces neither pairing nor axis-switching. Rather, as seen in Fig. 2 (a), along the minor axis plane, each pair of spanwise rollers is sucked in between the proceeding pair, thereby producing a reduction in width. Correspondingly, the pair of rollers, along the major axis plane are pushed out, thereby producing an increase in width in the plane. The net effect is opposite to the tendency towards axis-switching in the single mode case 1. In fact, Fig. 2 (e) shows that the jet is moving towards bifurcation. A similar phenomenon was observed by Zaman [12] in experiments in rectangular jets in which tabs were placed in the exit plane along the wider sides. In that case, the jet bifurcation was caused by the streamwise vorticity induced by the tabs, whereas in the present case, the streamwise vorticity inducing bifurcation, evolved naturally. Zaman also observed axis-switching, similar to our case 1, when the tabs were placed along the narrow sides of the rectangular plane. Hence, the natural processes simulated in cases 1 and 2 can be achieved experimentally by selective placement of tabs. In the presence of more sub-harmonic modes, the results in Fig. 3 show that self-induction will not lead to axis-switching. Thus natural jets at low Reynolds numbers, with a broad mode of disturbances in the shear layer are not expected to undergo axis-switching.

High Reynolds Number Jets

At higher Reynolds numbers, transition to turbulence occurs in the near field. There is then a competition between largely inviscid mechanisms and turbulent mechanisms in the subsequent evolution of the jet. The question is which mechanism dominates, under what conditions? Figures 4-6 show computed streamwise velocity for cases 4 to 6, respectively, which have been averaged over several time steps. We see clearly that axis-switching occurred in both the rectangular and the elliptic jets. The round jet, of course, remained circular with no preferential growth direction. Jet evolution can be explained with the mean streamwise vorticity equation:

$$0 = \underbrace{-U_1\frac{\partial\Omega_1}{\partial x_1}-U_2\frac{\partial\Omega_1}{\partial x_2}-U_3\frac{\partial\Omega_1}{\partial x_3}}_{A_1}\quad\underbrace{-\Omega_1\frac{\partial U_1}{\partial x_1}-\Omega_2\frac{\partial U_1}{\partial x_2}-\Omega_3\frac{\partial U_1}{\partial x_3}}_{A_2}$$
$$+\underbrace{\frac{\partial}{\partial x_1}\left(\frac{\partial\overline{u_1u_2}}{\partial x_3}-\frac{\partial\overline{u_1u_3}}{\partial x_2}\right)}_{A_3}+\underbrace{\frac{\partial^2}{\partial x_2\partial x_3}\left(\overline{u_3^2}-\overline{u_2^2}\right)}_{A_4}$$
$$\underbrace{-\left(\frac{\partial^2}{\partial x_3^2}-\frac{\partial^2}{\partial x_2^2}\right)\overline{u_2u_3}}_{A_5}+\underbrace{\frac{1}{\mathrm{Re}}\left(\frac{\partial^2}{\partial x_1}+\frac{\partial^2}{\partial x_2}+\frac{\partial^2}{\partial x_3}\right)\Omega_1}_{A_6}\quad\cdots\cdots\cdots(6)$$

where A_1 represents convection, A_2 vortex tilting and stretching, A_3 - A_5 are terms resulting from the anisotropy of turbulent stresses, and A_6 is the diffusion term. The last plays little role in high Reynolds number flows. Figure 7 shows the terms obtained by post-processing the LES results of case 4, at $x/D_e = 3.75$. The mean streamwise vorticity, Ω_1 and velocity, U_1 are also shown. (Negative values are shown as dashed lines.) This is the location at which streamwise vor-ticity starts to form and the distortion of the mean velocity contours from super-ellipses commences. It is clear that the two terms involving the

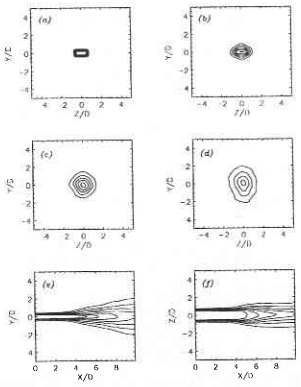

Figure 4. Contours of time-averaged streamwise velocity for LES of the rectangular jet, case 4; (a) $x/D_e = 0$, (b) $x/D_e = 4.88$, (c) $x/D_e = 7.31$, (d) $x/D_e = 9.755$, and (e) minor axis plane $z/D_e = 0$, (f) major axis plane, $y/D_e = 0$.

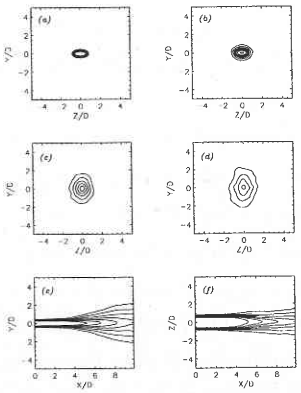

Figure 5. Contours of time-averaged streamwise velocity for LES of the elliptic jet, case 5 (See Figure 4 for Legend)

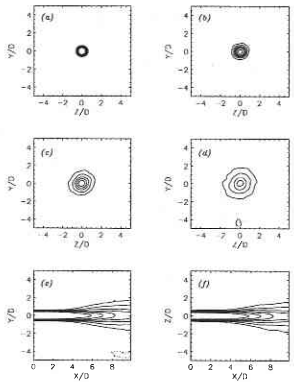

Figure 6. Contours of time-averaged streamwise velocity for LES of the round jet, case 6 (See Figure 4 for legend)

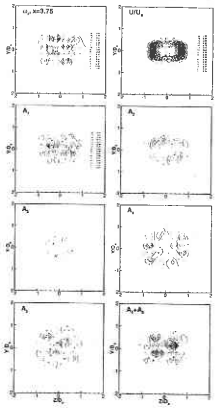

Figure 7. Balance of terms in the time-averaged streamwise vorticity equation for LES of the rectangular jet, case 4.

anisotropy of the secondary Reynolds stresses ($A_4 + A_5$) are responsible for the generation of the streamwise vorticity. They balance almost exactly the convection terms A_1. These are the same terms responsible for the generation of secondary motion in turbulent flow in non-circular ducts [13]. The inviscid, vortex tilting and stretching term, A_2 plays little or no role. *That is, for natural turbulent jets, with a broad-mode of instabilities in the shear-layer, jet evolution is controlled by turbulence-induced secondary motion, i.e., of Prandtl's second kind, and not by self-induction as in forced jets.* Hence, axis-switching in complex jets can be predicted with RANS, so long as the turbulence model utilized can reproduce the anisotropy of the turbulence. McGuirk and Rodi [9] had utilized a k-e turbulence model which is inadequate for this purpose. Therefore, their inability to predict axis-switching is not now surprising. Some form of Reynolds stress model (full or algebraic) would be required.

CONCLUDING REMARKS

Numerical simulation of jets with complex cross-sections have been performed using a third-order Runge-Kutta scheme for temporal integration and a fourth-order compact scheme for spatial discretization. Cases at low Reynolds numbers are direct simulations and those at high Reynolds number are large eddy simulations.

The phenomenon of axis-switching is observed to be dependent on instability waves present in the inlet boundary layers, and could be induced in both laminar and turbulent jets by single-mode forcing. It is confirmed that this is based on self-induction of the vorticity field. The presence of a discrete sub-harmonic modes led to its suppression and there was a tendency towards bifurcation.

Self-induction cannot produce axis-switching in jets which have a broad mode of instabilities in their shear layers. In non-turbulent jets, no axis-switching occurs. In turbulent jets, turbulence-induced secondary flow is responsible for axis-switching.

(Manuscript received, October 23, 1997)

REFERENCES

1) Ho, C.-M., and Gutmark, E., (1987) *J. Fluid Mech.*, Vol. 179, pp. 383-405.
2) Hussain, F. and Husain, H.S. (1989) *J. Fluid Mech.*, Vol. 208, pp. 257-320.
3) Quinn, W. R. (1989) *Phys. Fluid.* A, Vol. 1, No. 10, pp. 1716-1722.
4) Tsuchiya, Y., Horikoshi, C., Sato, T. and Takahashi, M. (1986) *JSME Int. J.*, II, 32, pp. 11-18.
5) Viets, H. and Sforza, P. M., (1972) *Phys-ics of Fluids*, Vol. 15, No. 2, pp. 230-240.
6) Dhanak, M. R. and DeBernandis, B., (1981) *Journal of Fluid Mechanics*, Vol. 100, pp. 189-216.
7) Koshigoe, S., Gutmark, E., Schadow, K.C., and Tubis, A., (1989) *AIAA Journal*, Vol. 27, pp. 411-419.
8) Tam, C. K. W. and Thies, A. T., (1993) *Journal of Fluid Mechanics*, Vol. 248, pp. 425-448.
9) McGuirk, J. J. and Rodi, W., (1979) In *Turbulent Shear Flows I*, Eds. F. Durst, B. E. Launder, F. W. Schmidt and J. H. Whitelaw, pp. 71-83.
10) Demuren, A.O., Wilson, R.V., Carpenter, M., and Kobayashi, T. (1998) *Seisan-Kenkyu*. Vol. 50.
11) Wilson, R. V. and Demuren, A. O. (1996) *Numerical Heat Transfer*, A., 29, pp. 485-509.
12) Zaman, K. B. M. Q., (1996) *Journal of Fluid Mechanics*, Vol. 316, pp. 1-27.
13) Demuren, A. O. and Rodi, W. (1984) *J. Fluid Mech.*, 140, pp. 189-222.